Published in final edited form as:

Mol Pharm. 2019 February 04; 16(2): 552–560. doi:10.1021/acs.molpharmaceut.8b00836.

3D Printing of Poloxamer 407 Nanogel Discs and Their Applications in Adjuvant Ovarian Cancer Therapy

Hyunah Cho[†,*], **Udayabhanu Jammalamadaka**[‡], **Karthik Tappa**[‡], **Christopher Egbulefu**[‡], **Julie Prior**[‡], **Rui Tang**[‡], **Samuel Achilefu**[‡]

[†] School of Pharmacy and Heath Sciences, Fairleigh Dickinson University, Florham Park, New Jersey 07932, United States

[‡] Mallinckrodt Institute of Radiology, Washington University School of Medicine, St. Louis, Missouri 63110, United States

Abstract

Nanogels are attractive biocompatible materials that enable local delivery of multiple drugs. In this study, we demonstrated that 3D printing technology could be used to precisely construct nanogel discs carrying paclitaxel and rapamycin. 3D-printed nanogel disc rounds (12 mm diameter × 1 mm thickness) carrying paclitaxel and rapamycin evaded premature gelation during storage and the initial burst release of the drugs in the dissolution medium. In vivo 3D-printed nanogel discs permitted successful intraperitoneal delivery of paclitaxel and rapamycin in ES-2-luc ovarian-cancer-bearing xenograft mice. They were also shown to be therapeutically effective and capable of preventing postsurgical peritoneal adhesions in the treated xenograft mice.

Graphical Abstract

[*]**Corresponding Author:** hyunahc@fdu.edu; Tel: 973-443-8234; Fax: 973-443-8431 (H.C.).

Author Contributions

The manuscript was written through contributions of all authors. All authors have given approval to the final version of the manuscript.

The authors declare no competing financial interest.

ASSOCIATED CONTENT

Supporting Information

The Supporting Information is available free of charge on the ACS Publications website at DOI: 10.1021/acs.molpharmaceut.8b00836.

3D printing of nanogels (AVI)

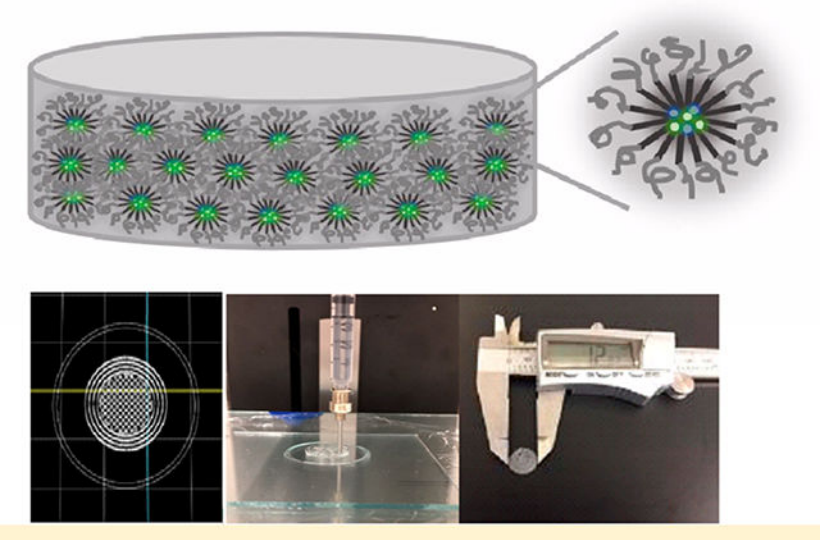

Keywords

3D printing; poloxamer; paclitaxel; ovarian cancer; peritoneal adhesion

INTRODUCTION

3D printing is a manufacturing method, in which solid or semisolid objects are built by fusing or depositing many thin layers.[1,2] 3D printing technology has been used in diverse fields, including architecture, fashion, and pharmaceutical/biomedical research. For example, various biomedical objects, such as tissues and organs, customized implants and prostheses, and anatomical models for surgical training, have been successfully 3D-printed. In the pharmaceutical field, various solid dosage forms, such as rapidly dissolving tablets, multilayered tablets, and caplet-in-caplet, have been constructed using 3D printing technology. In August 2015, the U.S. Food and Drug Administration (FDA) approved SPRITAM (Aprecia Pharmaceuticals, Blue Ash, OH), rapidly dissolving levetiracetam tablets for oral suspension manufactured using 3D printing technology.[3] SPRITAM disintegrates in the mouth with a sip of liquid within a few seconds and is offered for adjunctive therapy in the treatment of partial onset seizure, myoclonic seizures, and primary generated tonic-clonic seizures. SPRITAM, at the largest dose, i.e., 1000 mg, is a large tablet with a diameter of a nickel and a height of four nickels. While containing the large dose of levetiracetam, as a result of the porous nature of the tablet matrix, it rapidly disintegrates in the patient's mouth, making it easier to swallow. This new 3D-printed tablet product exemplifies that 3D printing technology can not only successfully build lab-scaled prototypes of solid dosage forms on-demand but also manufacture commercially acceptable products.

There are a number of 3D printing methods that can be used to create 3D objects, such as inkjet printing, selective laser sintering, fused deposition, and laminated object manufacturing.[4] Regardless of the types of printing methods, there is a basic procedure for

manufacturing 3D objects.[5] First, the object is designed in 3D using a software program. Second, the object design is converted to a readable format (e.g., STL file format) so that the program slices this object into printable layers and then transfers layer-by-layer instructions digitally to the printer. Third, raw materials are prepared as powders, granules, filaments, solutions, sols, or semisolids. Raw materials are added to the printing part or the extruder to build a desired construct. After printing, the object may go through the postprocessing steps such as drying, sintering, or polishing to give appealing aesthetics.

In this study, we used 3D printing technology, in particular, fused deposition technology, to construct a disc of poly(ethylene oxide)–*b*-poly(propylene oxide)–*b*-poly(ethylene oxide) (PEO-PPO-PEO) carrying paclitaxel and rapamycin. PEO-PPO-PEO is a triblock copolymer, commonly referred to as a poloxamer or by the trademarks Pluronic or Kolliphor, exhibiting thermally responsive properties. One of the poloxamers, poloxamer 407, has been widely used as a drug carrier, a thickening agent, and a hydrogel-based suspending medium. Micellization, multimolecular aggregates consisting of a hydrophobic core surrounded by hydrophilic chains facing the medium, occurs when the concentration of poloxamer 407 copolymers reaches the critical micelle concentration (CMC) at a given temperature.[6] At a higher concentration (20–30% w/w), above the critical gel concentration, micelles order themselves into a lattice. At an elevated temperature, hydrophilic chains of the copolymer are desolvated due to the breakage of the hydrogen bonds between the solvent and hydrophilic chains, leading to increased chain friction, hydrophobic chain association, and chain entanglement. In other words, at a low temperature, poloxamer 407 micelles are hydrated in water, resulting in free-flowing sols, and those enable incorporation of hydrophobic drugs in the hydrophobic core of micelles. At a higher temperature, for example, body temperature, i.e., 37 °C, poloxamer 407 micelles fuse together by leaching hydrophilic chains and enhancing the mechanical strength of the scaffold, resulting in gel formation. While a poloxamer 407 nanogel consisting of micellar networks is known to be one of the most promising local drug delivery systems and biomedical materials, it is also known to be inconvenient to store and handle and prone to induce burst-dissolution of the incorporated drugs because of the innate mechanical weakness. In this study, poloxamer 407 nanogels carrying paclitaxel and rapamycin were designed to be a thin 3D-printed disc to improve physical properties of the nanogels. Drug loading and elution of drugs were assessed in vitro, and the anticancer efficacy as an adjuvant chemotherapy and the preventive effect on postoperative peritoneal tissue adhesions were evaluated in ES-2-luc human ovarian-cancer-bearing xenograft mice in vivo. Postoperative peritoneal adhesions are known to greatly impact the quality of life of millions of patients who underwent peritoneal surgery worldwide.[7] Peritoneal adhesions are pathological bonds (thin films of connective tissues, thick fibrous bridges containing blood vessels, or a direct contact between two organ surfaces) made between the omenta, loops of bowel and the abdominal wall of the patients.[8] Peritoneal adhesions can cause major problems in patients including small bowel obstruction, chronic pelvic pain, dyspareunia, infertility, and higher complication rates in subsequent operations. Peritoneal adhesions can also be a cause of the mortality among the patients who underwent peritoneal surgery. The practical strategies currently used in the operating room to reduce postsurgical peritoneal tissue adhesions are minimization of operating time, irrigation of the abdominal cavity to remove residual blood depots, reduction

of infection risk by giving antibiotics, and use of moistened abdominal drapes or swabs or occasional application of saline to moist organ surfaces. Unfortunately, there have been no absolute solutions to prevent peritoneal adhesions, yet. In this study, poloxamer 407 nanogels carrying paclitaxel and rapamycin served as a disc-like device, preventing peritoneal adhesions after surgery and a treatment entity by eradicating residual tumor tissues.

MATERIALS AND METHODS

Preparation of Sol–Gels and Disks

Thermosensitive sol–gels using poloxamer 407 (kindly gifted by BASF, Tarrytown, NY) were prepared using a lyophilization method as previously described.[9] Briefly, poloxamer 407 (200 mg) dissolved in 1 mL of cold water (5 °C) was mixed with 1.1 mg of paclitaxel (LC Laboratories, Woburn, MA) and 1.1 mg of rapamycin (LC Laboratories, Woburn, MA) dissolved in 1 mL of *tert*-butanol (Sigma-Aldrich, St. Louis, MO) at 60 °C. The mixture was stored at −80 °C for 1 h and lyophilized for 24 h. The lyophilized cake was then rehydrated with 1 mL of cold DI water at 5 °C and gently stirred for 1 h in the cold room. The reconstituted sol was filtered through a 0.2 μm regenerated cellulose filter to remove unincorporated drugs and sterilize the rehydrated sol.

Discs were then prepared by using a Hyrel system 30 M standard resolution 3D printer (Hyrel 3D, Atlanta, Georgia). This closed 3D printing system was composed of a cold flow printing head (SDS-5), a heated stage (40 °C), a glass plate, a metal nozzle (0.84 mm in diameter, 18 gauge needle, suspended 0.2 mm above the glass plate), and a disposable sterile 1 or 3 mL syringe (kept cold at 10 °C). Sterile-filtered sol–gels with or without payloads were extruded from the disposable sterile syringe and deposited on the heated stage (disinfected with 70% isopropyl alcohol). Prior to printing, all parts including the printer windows, walls, a ceiling, and a bottom, were disinfected with 70% isopropyl alcohol. The layers of sol–gels were stacked at a 10 mm/s print speed under the linear motion control in X, Y, and Z axes. Each printed sol–gel round (360 μL of sols) was 16 mm in diameter and 2 mm in thickness. Sol–gels mounted on the glass plate were then dehydrated in the oven at 37 °C for 24 h. Final round disks were ca. 12 mm in diameter and ca. 1 mm in thickness.

Quantification of Paclitaxel and Rapamycin

Drug extraction for 3D-printed discs was performed to ensure that there was no notable amount of drugs adsorbed on the syringe/needle during the printing process. Briefly, a 3D-printed disc of nanogels carrying paclitaxel and rapamycin (360 μL) was dissolved in 10 mL of acetonitrile to extract the drugs. Similarly, sol–gels carrying paclitaxel and rapamycin (360 μL) were manually placed on the heated plate using a disposable sterile syringe/needle and a pipet. Manually extruded sol–gels were then dehydrated to form discs. A manually prepared disc carrying paclitaxel and rapamycin (360 μL) was dissolved in 10 mL of acetonitrile to extract the drugs. The levels of paclitaxel and rapamycin were detected using a liquid chromatograph mass spectrometer (LC-MS) system. A Shimadzu LCMS-2020 Single Quadrupole LC-MS (Columbia, MD, USA) was used to perform the LC-MS analysis using positive ion mode electrospray ionization (ESI) as the ion source with a source voltage

of 1.9 kV and capillary temperature of 300 °C. LabSolutions software (Shimadzu) was used for instrument control and data analysis. A Grace Vydac C18 HPLC (2.1 mm ID × 50 mm length, 3 μm particle size) was employed for LC separation using water with 0.1% trifluoroacetic acid (TFA) as the mobile phase A and acetonitrile with 0.1% TFA as the mobile phase B. The LC flow rate was set at 0.80 mL/min. The LC gradient increased from 5 to 95% mobile phase B in 6 min, held at 95% B for 2 min, returned to 5% B in 1 min, and then held at 5% B for 1 min. Paclitaxel and rapamycin were eluted separately from the LC column with baseline separation at a retention time of 4.6 min for paclitaxel (214 nm) and 5.7 min for rapamycin (254 nm). The areas under the curves representing paclitaxel and rapamycin were used to quantify the amounts of paclitaxel and rapamycin.

In Vitro Release Profiles for Sol–Gels and Discs

Sols and discs carrying paclitaxel and rapamycin, each measuring 360 μL, were placed in 100 mL of PBS stirred at 500 rpm, 37 °C (n = 4). At 0, 0.5, 1, 2, 3, 6, 12, and 24 h, 100 μL of PBS was removed. The rest of the PBS medium was removed and replaced with fresh PBS at regular intervals during the test periods. Collected PBS medium was used to quantify paclitaxel and rapamycin released from the gel matrices. The drug release profile was drawn on a first-order association using GraphPad Prism version 6 (La Jolla, CA).

Luciferase-Expressing ES-2 Human Ovarian Cancer Cells

ES-2 human ovarian cancer cells were cultured in McCoy's 5a medium supplemented with 1% L-glutamine, 10% fetal bovine serum, and 1% penicillin/streptomycin. ES-2 cells were transfected with luciferase-expressing plasmid pGL4.5.1 containing neomycin-resistance gene (Promega, Madison, WI) using a Lipofectamine 2000 transfection reagent (Thermo-fisher Scientific, Waltham, MA). After 48 h, ES-2 cells were cultured using the corresponding medium containing 750 μg/mL of G418 selective antibiotics for 3–4 weeks and 500 μg/mL of for another 3–4 weeks.

ES-2-luc-ascites mouse ovarian cancer cells were obtained by collecting ascites from peritoneal ES-2-luc-bearing nude mice. ES-2-luc cells (10^6 cells/animal) were injected into the peritoneal cavity 14 days prior to harvesting ascites. ES-2-luc-$PTX_{treated}$-ascites mouse ovarian cancer cells were obtained by collecting ascites from peritoneal ES-2-luc-bearing nude mice treated intraperitoneally with 20 mg/kg of paclitaxel 7 days prior to harvesting ascites. ES-2-luc-$PTX_{treated}$-ascites mouse ovarian cancer cells were used to assess a synergistic effect of paclitaxel and rapamycin in ES-2 ovarian cancer cells resistant to paclitaxel.

A linear relation between the number of cells and the intensity of bioluminescence expressed in ES-2-luc cells was confirmed using an IVIS 50 (PerkinElmer, Waltham, MA; Living Image 2.6, 1 min exposure, bin 8, FOV 12 cm, f/stop 1, open filter). D-Luciferin at 150 μg/mL was added to 96-well plates 10 min prior to bioluminescence imaging (data not shown).

Cell Cytotoxicity Study

In vitro cell cytotoxicity of paclitaxel and rapamycin, individually and in combination, was assessed in ES-2-luc human ovarian cancer cells, and ES-2-luc ascites mouse ovarian cancer cells and ES-2-luc-$PTX_{treated}$-ascites mouse ovarian cancer cells. ES-2-luc cells (5000 cells/well), ES-2-luc ascites cells (4000 cells/well), and ES-2-luc-$PTX_{treated}$ ascites cells (4000 cells/well) were placed in 96-well plates and incubated for 24 h. Paclitaxel and rapamycin (1:1 w/w) were added to the well plates at final drug concentrations of 0.1, 1, 10, 100, and 1000 nM, individually or in combination. Cell viability was determined 24 h post-treatment by quantifying the intensity of bioluminescence expressed in surviving cells. Cells were imaged using an IVIS 50 (1 min exposure, bin 8, FOV 12 cm, f/stop 1, open filter) 10 min after addition of 150 μg/mL of D-luciferin (Gold Biotechnology, St. Louis, MO). A grid was placed over the plate, and total photon flux (photons/sec) was measured from each well using Living Image 2.6.

The half inhibitory drug concentration (IC50), drug combination index (CI), and dose reduction index (DRI) for the synergy quantification were simulated using the medium-effect plot and the Fa-DRI plot) available in the CompuSyn software (Paramus, NJ).

In Vivo Human Ovarian Cancer Xenografts, Peritoneal Surgery, and Drug Administration

All animal studies were approved by the Washington University in St. Louis's Institutional Animal Care and Use Committee and conducted in accordance with the institutional and NIH guidelines.

Athymic NCr-nu/nu mice (6 weeks old, females) were obtained from Charles River Laboratories (Wilmington, MA). General anesthesia was induced with 1.5% isoflurane/oxygen and maintained with 1% isoflurane/oxygen. ES-2-luc human ovarian cancer cells (10^6 cells/animal) were suspended in 200 μL of PBS and injected intraperitoneally in anesthetized mice. Five days after cell inoculation, animals underwent peritoneal surgery for tumor resection unless otherwise noted. Peritoneal surgery was conducted in a double-blinded method to prevent outcomes from being biased. Briefly, all mice were injected with Buprenorphine SR (0.5 mg/kg) subcutaneously 1 h prior to the surgical procedure followed by intraperitoneal injection of a cocktail of ketamine (83.5 mg/kg) and xylazine (12.5 mg/kg) at the time of surgery. The depth of anesthesia was assessed using toe pinch. Skin preparation done by scrubbing skin with povidone–iodine-soaked gauze and sterile alcohol wipes. The mouse was then covered with a sterile drape. A 1.5 to 2 cm incision was made on the midline, abdominal wall (linea alba), and peritoneum. Intestine and organs were carefully lifted with forceps and blindly searched for the cancer cell niche. The identified cancer cell niche was carefully picked with sterile microdissection forceps and fine tip high-temperature cautery (Bovie Medical Corp., Purchase, NY). The exposed intestinal content was irrigated with a warm normal saline solution. Prior to the closure, the following formulations were placed on top of the abdominal organs below the peritoneum ($n = 5$): (i) empty discs; (ii) discs carrying paclitaxel and rapamycin; (iii) empty sol–gels; and (iv) sol–gels carrying paclitaxel and rapamycin. Abdominal cavity closure was done in two layers using an absorbable suture for continuous suturing of peritoneum and abdominal muscle and later using a monofilament nylon for interrupted closure of skin. Mice were kept in a clean

cage until recovery. In a control, ES-2-luc-bearing mice (n = 5) did not undergo surgical tumor resection and never received any treatment. Animals were monitored at least daily in 3 days postsurgery and weekly afterward; a postoperation monitoring form was filled out to examine and record the health conditions of mice. Whole-body bioluminescence images were obtained at days 1, 3, 7, 14, 21, 28, 35, and 42 days postsurgery to determine tumor progression/regression. Animals were euthanized at the time of reaching a moribund condition. Euthanized animals were monitored with their peritoneal conditions including peritoneal adhesion, amount of peritoneal ascites, color of ascites fluids, and size of tumor tissues.

In Vivo Whole-Body Bioluminescence Imaging

In vivo bioluminescence imaging was performed on the days indicated on an IVIS Lumina (PerkinElmer, Waltham, WA; Living Image 3.2, 1 to 60 s exposure, bin 2–8, FOV 12.5 cm, f/stop 1, open filter). Mice were injected intraperitoneally with D-luciferin (150 mg/kg in PBS; Gold Biotechnology, St. Louis, MO), and 10 min later, they were imaged using isoflurane anesthesia (2% vaporized in oxygen). Total photon flux (photons/sec) was measured from the fixed regions of interest (ROIs) over the mouse abdomen using Living Image 2.6.

RESULTS

Characterizations of Sol–Gels and Discs Carrying Paclitaxel and Rapamycin

Figure 1 presents a brief procedure of preparing sol–gels and discs (Supporting Information) carrying paclitaxel and rapamycin. The 3D printer was programmed to build a round with 16 mm diameter and 2 mm thickness. Three rounds were printed on the glass plate in a single printing setting. Gel discs were then dehydrated in an oven at 37 °C for 24 h. The resulting discs were 12 ± 0.3 mm in diameter and 1 ± 0.02 mm in thickness with a smooth circular surface. Discs weighed 109 ± 1 mg. When the PBS buffer was added to the discs at 37 °C, the discs absorbed the buffer and gradually turned into gels. For instance, when a single disc (12 mm in diameter and 1 mm in thickness) was immersed in 10 mL of the PBS buffer, a complete disc-to-gel transition occurred in ca. 40 min. Nanogels made a successful sol–gel transition driven by temperature change (sol at 5 °C and gel at 37 °C). A sol turned into a gel at 37 °C in ca. 2 min. The amounts of paclitaxel and rapamycin incorporated in the sol–gels and discs were approximately 99 ± 1% ([drugs incorporated]/[drugs added] × 100). The drug extraction result (comparing 3D-printed vs manually extruded discs carrying paclitaxel and rapamycin) indicated that there was no notable amount of drugs adsorbed or adhered onto the parts of the printer.

Figure 2 shows release profiles of paclitaxel and rapamycin for the sol–gels and discs. Release profiles of paclitaxel and rapamycin for sol–gels were fit into two-phase associations (R^2 = 0.8412 and 0.9002, respectively) whereas those for discs were fit into one-phase associations (R^2 = 0.9166 and 0.9049, respectively). For sol–gels, in 30 min at 37 °C, ca. 33% of paclitaxel and ca. 39% of rapamycin were released, and after 6 h, ca. 50% of paclitaxel and ca. 61% rapamycin were released. At the 24 h time point, ca. 62% of paclitaxel and ca. 86% of rapamycin were released from sol–gels into the buffer, which

draws the biphasic drug release pattern. For discs, in 30 min at 37 °C, ca. 14% of paclitaxel and 20% of rapamycin were eluted, and after 6 h, ca. 38% of paclitaxel and 51% rapamycin were eluted. At the 24 h time point, ca. 60% of paclitaxel and 82% of rapamycin were eluted from discs in the one-phase drug release pattern.

In Vitro Cytotoxicity Study

Table 1 presents IC_{50} values of paclitaxel and rapamycin, individually and in combination, in ES-2-luc human ovarian cancer, ES-2-luc-ascites mouse cancer cells, and ES-2-luc-$PTX_{treated}$-ascites mouse cancer cells. Paclitaxel alone was effective in killing ES-2-luc-derived ovarian cancer cells. To evaluate the synergistic effect of paclitaxel and rapamycin in combination, a combination index (CI) was calculated. CI < 1, = 1, or > 1 indicates synergism, an additive effect, or antagonism, respectively.

On the basis of the CI values (Table 1), the highest synergism induced by a combination of paclitaxel and rapamycin was shown in treating paclitaxel-resistant ES-2-luc ascites mouse ovarian cancer cells (CI 0.2368).

In ES-2-luc human ovarian cancer cells, synergism (CI < 1) at Fa ≥ 0.36 (Fa: the ratio of the fraction affected) was estimated, and the simulation at low Fa showed substantial antagonism (CI > 1). It indicates that synergism (CI < 1) at high dose is more relevant to the therapy than the CI values at low dose. On the basis of the dose reduction index (DRI, a measure of how many folds the dose of each drug in a synergistic combination may be reduced in comparison to the dose of each drug alone) at 50% cell inhibition, it permits 1.83-fold less paclitaxel plus 9.94-fold less rapamycin when combined. In ES-2-luc-ascites mouse cancer cells (obtained from the ascites collected from ES-2-luc ovarian cancer xenograft mice), at Fa ≥ 0.25, it showed synergist effects, while the low dose of paclitaxel and rapamycin may not cause synergism. It allows 5.09-fold less paclitaxel plus 20.49-fold less rapamycin as a combination to induce 50% cell inhibition. Interestingly, in ES-2-luc-$PTX_{treated}$-ascites mouse cancer cells (obtained from the ascites collected in paclitaxel-treated ES-2-luc ovarian cancer xenograft mice), synergism was estimated at 0.15 ≤ Fa ≤ 0.9, indicating that a paclitaxel–rapamycin combination at high dose as well as low dose may not be therapeutically synergistic. At 50% cell inhibition (within the range of synergism), it allows 5.92-fold less paclitaxel plus 14.74-fold less rapamycin when combined. The information collected here implies that the intermediate dose of paclitaxel and rapamycin is recommended in treating paclitaxel-resistant ES-luc cancer cells, whereas the high dose of paclitaxel and rapamycin is synergistically effective in treating ES-2-luc cancer cells.

In Vivo Anticancer Efficacy of Discs Carrying Paclitaxel and Rapamycin and Their Preventive Effect on Postoperative Peritoneal Adhesion in ES-2-luc-Bearing Xenograft Mice

The anticancer efficacy of paclitaxel and rapamycin intraperitoneally delivered via poloxamer 407 in discs and in sol–gels was evaluated in ES-2-luc human ovarian-cancer-bearing xenograft mice. Tumor progression was monitored by detecting bioluminescent tumor tissues and cells via scanning whole-body bioluminescence images longitudinally.

To simulate intraperitoneal surgery followed by adjuvant therapy, first, a small incision was made on the abdominal skin of nude mice with peritoneal ES-2-luc ovarian cancer to get access to the peritoneal cavity (Figure 3). Surgery was carefully performed to remove as many tumor tissues as possible. In general, tumor tissues were identified as thick white lesions on the surfaces and walls of intestines, mesentery, and especially around the spleen. Tumors invading the intestinal wall were cauterized, and mesenteric lesions were excised with minimal bleeding.

The tumor burden of the mice who underwent tumor reduction surgery followed by intraperitoneal insertion of a single disc carrying paclitaxel and rapamycin (20/20 mg/kg) decreased substantially from ca. 100 to ca. 30% a day postprocedure and subsequently decreased down to ca. 20% 3 days postprocedure (Figure 4). At day 7 postprocedure, tumor burden increased to ca. 69%. At day 14, tumor burden increased to ca. 804%. At day 28, tumor burden notably increased, reaching 4250% with the buildup of ascites (fluid accumulation within the abdomen leading to potbellied appearance). The median survival of animals in this group of five mice was 30 days (Figure 5 and Table 2).

The tumor burden of ES-2-luc-bearing mice who received a cold sol carrying paclitaxel and rapamycin (20/20 mg/kg) intraperitoneally after surgery also showed a notable decrease in tumor burden from ca. 100 to ca. 52% a day postprocedure and continued to decrease to ca. 35% at day 3. At day 7, the tumor regrew substantially and reached ca. 131% in tumor burden, which is slightly greater than that at day 0 just prior to surgery. By day 28, the tumor progressed rapidly, reaching ca. 2215% with a noticeable abdominal mass at day 14, ca. 45 281% at day 21, and ca. 283 936% with a large abdominal mass at day 28. The median survival of animals in this group of five mice was 36 days.

Peritoneal surgery, in the beginning, helped decrease tumor burden in ES-2-luc-bearing mice (from ca. 100 to ca. 21% at day 1) who received an empty disc without drugs after surgery. However, the ES-2-luc tumor continuously increased to ca. 136% at day 3, ca. 3011% at day 7, ca. 11 767% at day 14, and 145 308% with large abdominal fluid buildup at day 28. The median survival of animals in this group of five mice was 21 days. Similarly, tumor burden decreased from 100 to ca. 28% after surgery at day 1 but soon significantly increased to 153% at day 3, ca. 934% at day 7, ca. 21 039% at day 14, and ca. 61 368% at day 21 in ES-2-luc-bearing mice who received an empty sol–gel after surgery. The median survival of animals in this group was 21 days.

In a control group of five mice who did not receive any surgical procedure and treatment, continuously increased tumor burden from ca. 100 to ca. 169% at day 1, ca. 390% at day 3, ca. 1223% at day 7, and 6162% at day 14 was observed. The median survival of animals in this control group was 21 days.

Figure 6 and Table 3 demonstrate peritoneal presentations of mice associated with cancer and/or adjuvant therapy. The normal appearance of peritoneal fluids is considered to be straw-colored and clear. Abnormal appearances give clues to health conditions and a disease status. There was a notable postoperative peritoneal adhesion between the peritoneal wall and the gastrointestinal organs in four out of five ES-2-luc-bearing mice treated with an

empty sol–gel. The stomach and parts of the ileum adhered to the peritoneal wall. Mice in the control group presented the largest amount of peritoneal fluids, which were milky and cloudy, indicating that there was a presence of white blood cells, infection, lymph system blockage, or trauma. Peritoneal tumor tissues were various in texture in mice in the control group: There were large solid tumor tissues (>1 cm in diameter) found on the peritoneal wall and near the duodenum and spleen. Small soft tumor tissues (<0.3 cm in diameter) were disseminated onto the ileum, mesentery, uterus, cecum, ovary, omental fat, pancreas, liver, and even heart. Small liquid-like tumor tissues were also found on the stomach, ileum, colon, jejunum, and duodenum. Mice treated with sol–gels with paclitaxel and rapamycin or with an empty sol–gel presented pinkish and slightly cloudy peritoneal fluids as a result of the presence of blood most likely due to the surgery-associated trauma. Peritoneal fluids in mice treated with discs carrying paclitaxel and rapamycin were straw-colored ($n = 3$) or yellow ($n = 2$), indicating that two out of five mice possibly had issues associated with functionality of the liver. Those two mice with yellow peritoneal fluids also had enlarged gallbladders, an indicator of hepatic dysfunction.

DISCUSSION

Thermosensitive hydrogels are attractive biocompatible materials, which enable depot delivery of multiple drugs by forming gels in the patient's body, absorbing body fluids to swell, and gradually releasing payloads at the site of application.[10] As a result of this temperature-responsive behavior, biomedical applications of various hydrogels have been explored in the areas of regeneration medicine and cancer therapy. In particular, poloxamer 407, a hydrophilic triblock copolymer composed of one hydrophobic poly(propylene oxide) block and two hydrophilic poly(ethylene oxide) side chains, has been widely used to delivery drugs locally. Poloxamer 407 can make a transition from a sol to a gel through micellization followed by aggregation at an elevated temperature.[11] As a result of the micelle-forming structure of poloxamer 407, it has shown to be one of the promising drug delivery carriers useful in personalized medicine and novel biomedical applications. While poloxamer 407-based hydrogels have several advantages as a drug delivery system, there are a few limitations. One of the major limitations is inconvenience in handling and manufacturing, which demands more efforts on sophisticated manufacturing method development. 3D printing in the pharmaceutical field represents an elegant tool for designing simple, accurate, and inexpensive drug delivery systems.[12] Recent advancements in the 3D printing technology have led to achieving high precision, high efficiency, and convenient operations, which permits creating patient-specific and rationally designed biomedical materials or devices. In this study, we used a nozzle-based deposition 3D printing system, where the components were prepared as a mixture prior to 3D printing. This system deposited poloxamer 407 sols carrying paclitaxel and rapamycin directly through a nozzle (kept at 10 °C) onto the heated glass plate (40 °C) to create a 3D layer-by-layer pattern with controlled composition and architecture. Extruded gels were then dehydrated into thin solid discs, permitting convenient handling and storage at room temperature, whereas sols required low-temperature storage conditions to avoid premature gelation followed by the burst release of drugs. In the clinical settings, healthcare providers pick up a disc and place it in the patient's peritoneal cavity just prior to the peritoneal closure without any concerns of

unsuccessful delivery of medications caused by the needle blockage. Furthermore, insertion of discs does not alter the patient's body temperature, whereas administration of cold sols quickly lowers body temperature, which may affect postsurgical recovery. Here, we were able to design and create an extruded gel disc of poloxamer 407 carrying paclitaxel and rapamycin (16 mm in diameter and 2 mm in thickness) and dehydrated it to be a solid disc (12 mm in diameter and 1 mm in thickness), which is smaller than a dime. This was customized to be small enough to fit in the peritoneal cavity of mice and large enough to cover the interface between the surgical incisions and the internal organ to serve as a physical barrier. It proves that the 3D printing technology permitted precise fabrication of small objects. If needed, the shape, thickness, and diameter of the objects can be easily modified using the 3D printing technology on-demand, potentially being an important tool for personalized medicine.

On the basis of the release profiles of paclitaxel and rapamycin, it appears that sol–gels carrying paclitaxel and rapamycin showed burst release in the first few hours and then decreased release of drugs thereafter. Discs carrying paclitaxel and rapamycin did not show the rapid burst release of drugs in the beginning. After 12 h, the amounts of drugs released from sol–gels and discs became almost identical. Presumably, it is because it takes an additional ca. 40 min for each disc to absorb the buffer solution to form gels. This evades one of the disadvantages of poloxamer 407 gels associated with the burst release of drugs and rapid erosion. Sol–gels composed of poloxamer tend to go through rapid erosion in the physiological environment because of microdilution in the patient's body, causing the poloxamer concentration to rapidly decrease and drop below the critical gelation concentration. Without additions of other polymers, surfactants, or solvents, we were able to avoid the burst release effect simply by making it into a disc. Regardless of the type of drug delivery vehicles, rapamycin (log P 4.3; water solubility 5 μM), a relatively more hydrophobic drug, showed a more rapid release pattern than did paclitaxel (log P 3.0; water solubility 10–20 μM). The release pattern of paclitaxel and rapamycin for poloxamer 407 gels (release rate: rapamycin > paclitaxel) was different from that of paclitaxel and rapamycin from PLGA-PEG-PLGA gels (identical release rate). It is presumed that the higher hydrophilicity of the poloxamer 407 gel matrix held the relatively more hydrophilic paclitaxel slightly longer, while rapamycin precipitated in the medium.[9]

Paclitaxel and rapamycin in combination has shown to synergistically target the PI3K/Akt/mTOR pathway by suppressing feedback loop Akt phosphorylation, resulting in improved inhibition of cell proliferation and apoptosis in various cancers including breast and endometrial cancers.[13–15] It appears that a combination of paclitaxel and rapamycin is also synergistically effective in killing paclitaxel-resistant ES-2-luc human ovarian cancer cells in vitro, particularly at the moderate total drug concentration.

Surgery is the cornerstone of treating ovarian cancer during advanced stages, noting that the size of the residual tumors after optimal debulking surgery substantially impacts longevity of the patients.[16,17] Women with advanced ovarian cancer are primarily managed with peritoneal surgery and subsequent conventional chemotherapy. Although performing a laparotomy is an inevitable process, many patients suffer from the postsurgical side effect known as peritoneal tissue adhesions. Peritoneal adhesions are mostly induced by surgical

procedures in the peritoneal cavity, and their prevalence after major abdominal procedures has reached 63–97%.[18] Overall, approximately one-third of the patients who underwent open abdominal surgery were readmitted an average of two times over the subsequent 10 years for conditions directly related to adhesions. Peritoneal adhesions represent an important clinical challenge in peritoneal surgery of gynecological patients.[18] Peritoneal adhesions are a consequence of peritoneal irritation by infection or surgical trauma. Those can be a major cause of morbidity, resulting in multiple complications. Consequences and complications of postsurgical peritoneal adhesions include small bowel obstruction, secondary infertility, and chronic abdominal and pelvic pain. Peritoneal adhesions also negatively impacted patient's wellbeing and socioeconomic costs.[7] Unfortunately, peritoneal adhesions have been underexposed in the literature, and there has been no definitive strategy to prevent their formulation. In this study, we simulated peritoneal surgery of advanced ovarian cancer patients and intraperitoneal administration of adjuvant chemotherapy (paclitaxel and rapamycin) in forms of a solution, a sol–gel, a gel-spread, and a nanogel disc. The rationale behind the intraperitoneal adjuvant therapy is that longer exposure of cytotoxic drugs and cytotoxic drugs directly targeting tumor masses confined to the abdominal cavity can be achieved while reducing the systemic toxicity.[19–21] ES-2-luc human ovarian-cancer-bearing mice underwent peritoneal surgery to remove tumor tissues, and a disc and a sol–gel with or without drugs were placed to eliminate residual tumor tissues and cells after surgery and hinder formations of postsurgical peritoneal adhesions by minimizing direct contact between the damaged serosal surface and abdominal organs. ES-2-luc human ovarian-cancer-bearing mice showed the least amount of bioluminescent ES-2-luc cells in the body after an intraperitoneal insertion of a disc carrying paclitaxel and rapamycin at 20/20 mg/kg. When it comes to inducing a reduction in bioluminescent signals emitted by residual cancer cells, a sol–gel carrying paclitaxel and rapamycin was not as effective as a disc carrying those. Although a disc carrying paclitaxel and rapamycin notably decreased tumor burden in mice, the median survival of mice was 6 days shorter than those treated with a sol–gel carrying paclitaxel and rapamycin. The reason was found after exploring the peritoneum and internal organs of euthanized animals. Peritoneal ascites of two mice treated with a disc carrying paclitaxel and rapamycin were prominently yellow in color, indicating the presence of liver problems. The remaining three mice treated with a disc carrying paclitaxel and rapamycin were straw-colored (considered normal). Clinically, it has been reported that in some patients who have been treated with albumin-bound paclitaxel (nab-paclitaxel, Abraxane), transient elevation of alkaline phosphatase, aspartate aminotransferase, and bilirubin have been reported in approximately 40% of cases.[22,23] Patients with slightly elevated alkaline phosphatase or aspartate aminotransferase may decrease paclitaxel clearance and are at increased risk of therapy-related toxicity. The impact of hepatic dysfunction on paclitaxel clearance varies depending on the duration of drug infusion; therefore, for Abraxane, it is recommended to reduce initial doses in patients with hepatic impairment. Similarly, in our study, it appears that there was hepatic dysfunction in two mice treated with a disc carrying paclitaxel and rapamycin. It may be because a disc allowed drugs to remain in the peritoneal cavity for a longer time, whereas a sol–gel more rapidly degraded and lost drugs. Considering that a disc with drugs induced substantially superior therapeutic efficacy to a sol–gel with drugs at the same concentration, dose adjustment for a

disc formulation must be made for the future study to improve therapeutic activities while avoiding hepatic impairment.

Empty sol–gels failed to separate the damaged peritoneal wall from the abdominal organs. Four mice treated with empty sol–gels developed severe peritoneal adhesions. It was noted that a sol distributed on top of the organs was moved deeper into the gaps between the gastrointestinal organs without remaining as a thin film because of the greater flowability. As intraperitoneal insertion of cold sols decreased the temperature of mice; animals shivered as a result of being cold after recovery. Unlike mice treated with empty sol–gels, mice treated with sol–gels carrying paclitaxel and rapamycin did not have postsurgical peritoneal adhesions. It is because some chemical agents prevent the organization of the persisting fibrin, such as nonsteroidal anti-inflammatory drugs (NSAIDs), antibiotics, chemotherapeutics (e.g., paclitaxel) and immunosuppressors (e.g. rapamycin).[24] Empty discs and discs carrying paclitaxel and rapamycin completely prevented postsurgical peritoneal adhesions in treated xenograft mice. Presumably, empty discs helped avoid peritoneal adhesions without any chemical agents, because empty discs made a gradual transition into gels in the small amount of peritoneal fluids, resulting in a longer residence time as a physical barrier on the peritoneal surface.

CONCLUSION

3D printing technology was well-suited for convenient preparation of a poloxamer 407 nanogel disc carrying paclitaxel and rapamycin. 3D-printed discs carrying drugs permitted easy handling, successful peritoneal delivery of drugs, prevention of postsurgical peritoneal adhesion, and increase in survival of ovarian-cancer-bearing xenograft mice. Paclitaxel and rapamycin concurrently delivered via a nanogel disc in vivo may be adjusted to be lower in concentrations to avoid hepatic toxicity.

Supplementary Material

Refer to Web version on PubMed Central for supplementary material.

ACKNOWLEDGMENTS

This study was supported by a St. Louis College of Pharmacy Faculty Research Incentive Fund, NIH P50 CA094056, and a Fairleigh Dickinson University Provost Seed Grant.

REFERENCES

(1). Goyanes A; Wang J; Buanz A; Martinez-Pacheco R; Telford R; Gaisford S; Basit AW 3D Printing of Medicines: Engineering Novel Oral Devices with Unique Design and Drug Release Characteristics. Mol. Pharmaceutics 2015, 12 (11), 4077–84.

(2). Ventola CL Medical Applications for 3D Printing: Current and Projected Uses. P T 2014, 39 (10), 704–711. [PubMed: 25336867]

(3). Spritam--a new formulation of levetiracetam for epilepsy. Med. Lett. Drugs Ther 2016, 58, (1497), 78–79. [PubMed: 27305068]

(4). Gross BC; Erkal JL; Lockwood SY; Chen C; Spence DM Evaluation of 3D printing and its potential impact on biotechnology and the chemical sciences. Anal. Chem. 2014, 86 (7), 3240–53. [PubMed: 24432804]

(5). Norman J; Madurawe RD; Moore CM; Khan MA; Khairuzzaman A A new chapter in pharmaceutical manufacturing: 3D-printed drug products. Adv. Drug Delivery Rev. 2017, 108, 39–50.

(6). Escobar-Chavez JJ; Lopez-Cervantes M; Naik A; Kalia YN; Quintanar-Guerrero D; Ganem-Quintanar A Applications of thermo-reversible pluronic F-127 gels in pharmaceutical formulations. J. Pharm. Pharm. Sci 2006, 9 (3), 339–358. [PubMed: 17207417]

(7). van Goor H Consequences and complications of peritoneal adhesions. Colorectal Dis 2007, 9 (s2), 25–34. [PubMed: 17824967]

(8). Bruggmann D; Tchartchian G; Wallwiener M; Munstedt K; Tinneberg HR; Hackethal A Intra-abdominal adhesions: definition, origin, significance in surgical practice, and treatment options. Dtsch Arztebl Int. 2010, 107 (44), 769–775. [PubMed: 21116396]

(9). McKenzie M; Betts D; Suh A; Bui K; Tang R; Liang K; Achilefu S; Kwon GS; Cho H Proof-of-Concept of Polymeric Sol–Gels in Multi-Drug Delivery and Intraoperative Image-Guided Surgery for Peritoneal Ovarian Cancer. Pharm. Res. 2016, 33 (9), 2298–306. [PubMed: 27283829]

(10). McKenzie M; Betts D; Suh A; Bui K; Kim LD; Cho H Hydrogel-Based Drug Delivery Systems for Poorly Water-Soluble Drugs. Molecules 2015, 20 (11), 20397–408. [PubMed: 26580588]

(11). Ju C; Sun J; Zi P; Jin X; Zhang C Thermosensitive micelles-hydrogel hybrid system based on poloxamer 407 for localized delivery of paclitaxel. J. Pharm. Sci. 2013, 102 (8), 2707–17. [PubMed: 23839931]

(12). Goole J; Amighi K 3D printing in pharmaceutics: A new tool for designing customized drug delivery systems. Int. J. Pharm. 2016, 499 (1–2), 376–394. [PubMed: 26757150]

(13). Blanco E; Sangai T; Wu S; Hsiao A; Ruiz-Esparza GU; Gonzalez-Delgado CA; Cara FE; Granados-Principal S; Evans KW; Akcakanat A; Wang Y; Do KA; Meric-Bernstam F; Ferrari M Colocalized delivery of rapamycin and paclitaxel to tumors enhances synergistic targeting of the PI3K/Akt/mTOR pathway. Mol. Ther. 2014, 22 (7), 1310–9. [PubMed: 24569835]

(14). Shafer A; Zhou C; Gehrig PA; Boggess JF; Bae-Jump VL Rapamycin potentiates the effects of paclitaxel in endometrial cancer cells through inhibition of cell proliferation and induction of apoptosis. Int. J. Cancer 2009, 126 (5), 1144–1154.

(15). Tian W; Liu J; Guo Y; Shen Y; Zhou D; Guo S Self-assembled micelles of amphiphilic PEGylated rapamycin for loading paclitaxel and resisting multidrug resistant cancer cells. J. Mater. Chem. B 2015, 3 (7), 1204–1207. [PubMed: 25717377]

(16). Aletti GD; Gallenberg MM; Cliby WA; Jatoi A; Hartmann LC Current management strategies for ovarian cancer. Mayo Clin. Proc. 2007, 82 (6), 751–770. [PubMed: 17550756]

(17). Berek JS; Hacker NF; Lagasse LD; Nieberg RK; Elashoff RM Survival of patients following secondary cytoreductive surgery in ovarian cancer. Obstet Gynecol 1983, 61 (2), 189–193. [PubMed: 6823360]

(18). Arung W; Meurisse M; Detry O Pathophysiology and prevention of postoperative peritoneal adhesions. World J. Gastroenterol 2011, 17 (41), 4545–53. [PubMed: 22147959]

(19). Cho H; Kwon GS Thermosensitive poly-(d,l-lactide-co-glycolide)-block-poly(ethylene glycol)-block-poly-(d,l-lactide-co-glycolide) hydrogels for multi-drug delivery. J. Drug Target 2014, 22 (7), 669–77. [PubMed: 24964052]

(20). Cho H; Lai TC; Kwon GS Poly(ethylene glycol)-block-poly(epsilon-caprolactone) micelles for combination drug delivery: evaluation of paclitaxel, cyclopamine and gossypol in intraperitoneal xenograft models of ovarian cancer. J. Controlled Release 2013, 166 (1), 1–9.

(21). Fagotti A; Gallotta V; Romano F; Fanfani F; Rossitto C; Naldini A; Vigliotta M; Scambia G Peritoneal carcinosis of ovarian origin. World J. Gastrointest Oncol 2010, 2 (2), 102–8. [PubMed: 21160928]

(22). Biakhov MY; Kononova GV; Iglesias J; Desai N; Bhar P; Schmid AN; Loibl S nab-Paclitaxel in patients with advanced solid tumors and hepatic dysfunction: a pilot study. Expert Opin. Drug Saf. 2010, 9 (4), 515–23. [PubMed: 20500029]

(23). Vishnu P; Roy V Safety and Efficacy of nab-Paclitaxel in the Treatment of Patients with Breast Cancer. Breast Cancer: Basic Clin. Res. 2011, 5, 53–65.

(24). Maciver AH; McCall M; James Shapiro AM Intra-abdominal adhesions: cellular mechanisms and strategies for prevention. Int. J. Surg 2011, 9 (8), 589–94. [PubMed: 21964216]

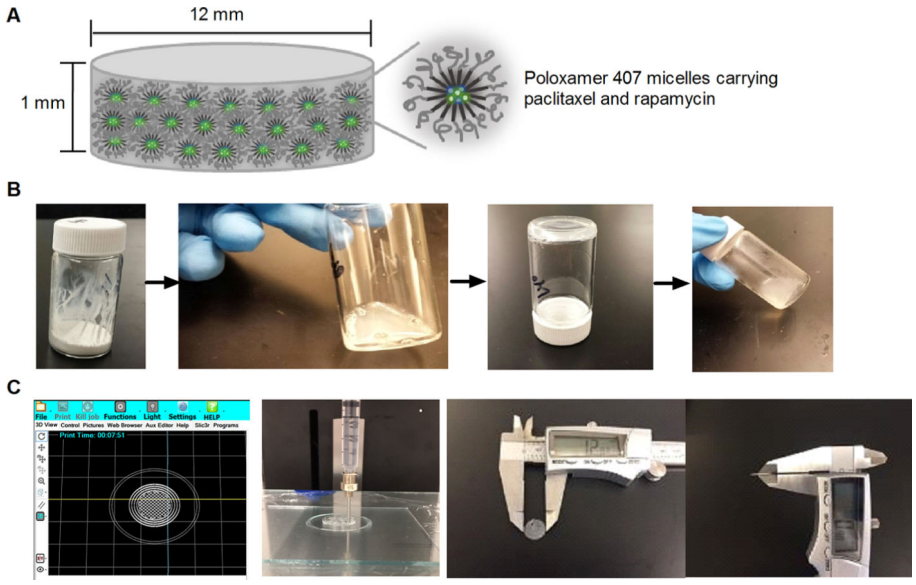

Figure 1.
Schematic illustration of a nanogel disc carrying paclitaxel and rapamycin (A) and a brief procedure for preparing sol–gels (B) and discs (C).

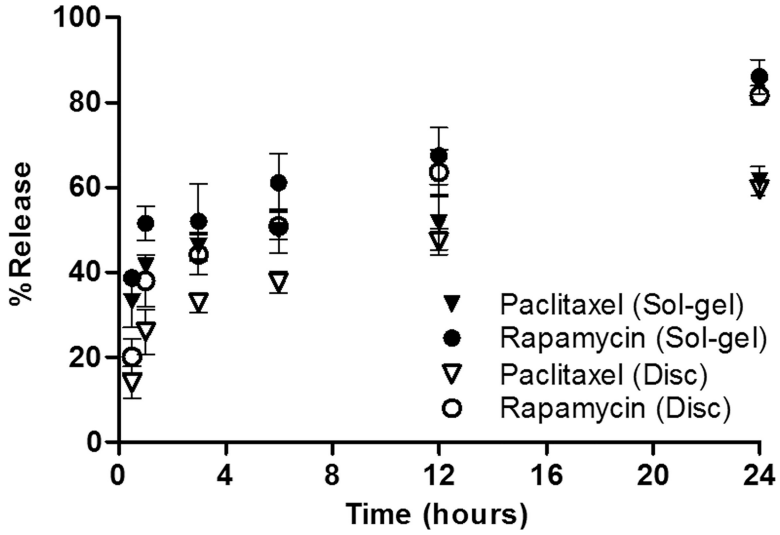

Figure 2.

Release profiles of paclitaxel and rapamycin for sol–gels and discs. Paclitaxel (Sol–gel) vs Paclitaxel (Disc): 30 min**, 1 h**, 3 h**, 6 h* and Rapamycin (Sol–gel) vs Rapamycin (Disc): 30 min**, 1 h* (*$p < 0.05$ and **$p < 0.01$).

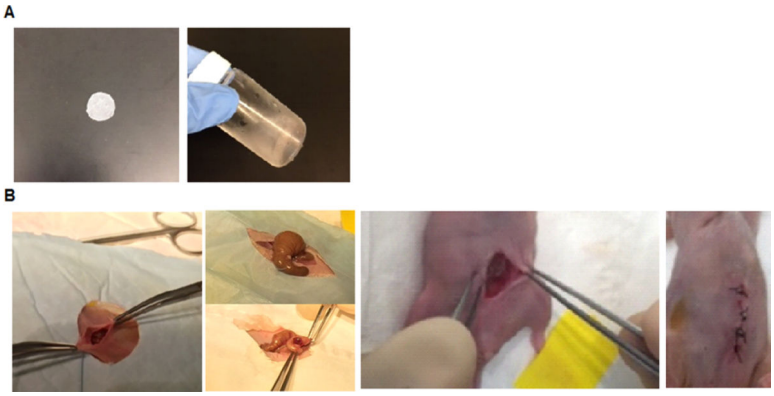

Figure 3.
Disc and sol–gel carrying paclitaxel and rapamycin (A) and surgical procedure in ES-2-luc-bearing xenograft mice (B).

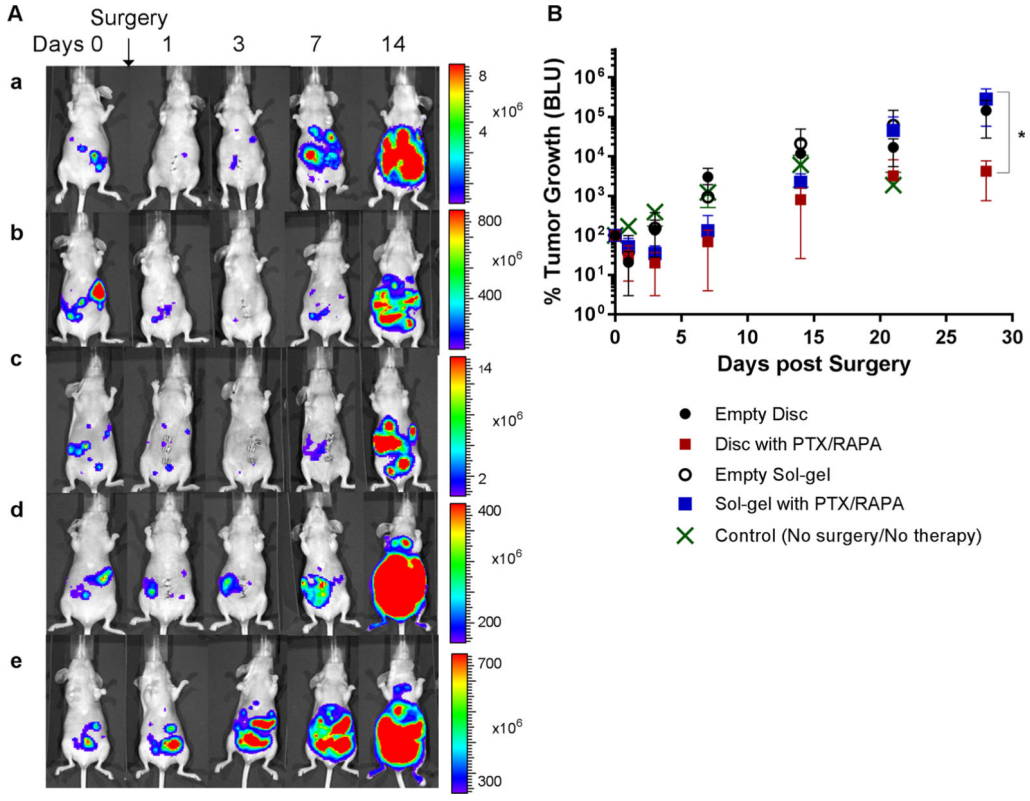

Figure 4.

In vivo whole-body bioluminescence images of ES-2-luc-bearing xenograft mice treated with the following: (a) surgery followed by insertion of an empty disc; (b) surgery followed by insertion of a disc carrying paclitaxel and rapamycin; (c) surgery followed by insertion of a sol–gel carrying paclitaxel and rapamycin; (d) surgery followed by insertion of an empty sol–gel; (e) control (no surgery and no treatment) (A) and in vivo tumor progression calculated based on the bioluminescence signals in ROIs (B) (*$p < 0.05$).

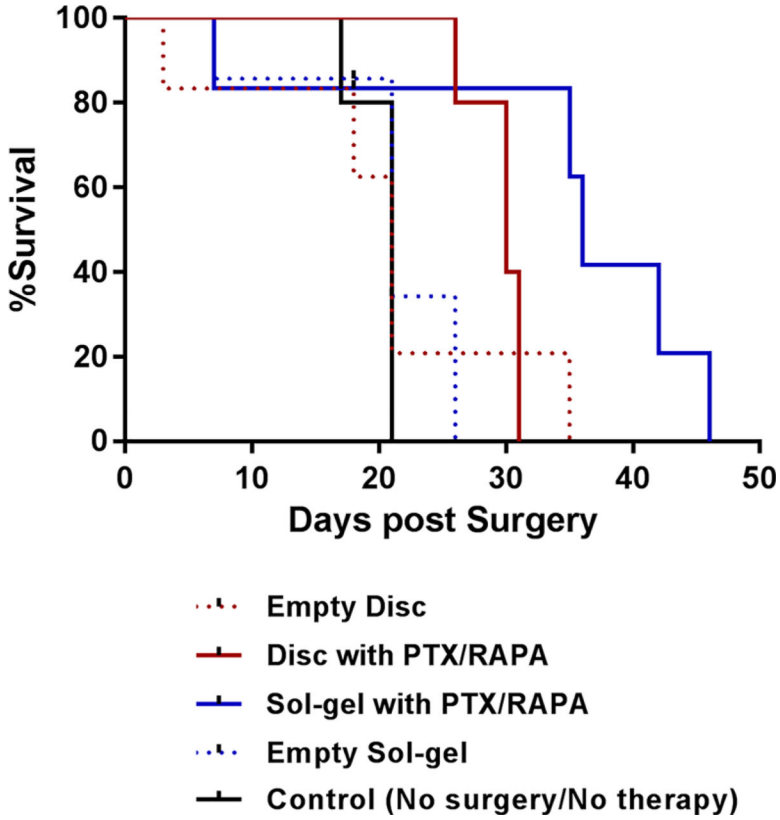

Figure 5.
Kaplan–Meier analyses for animal survival.

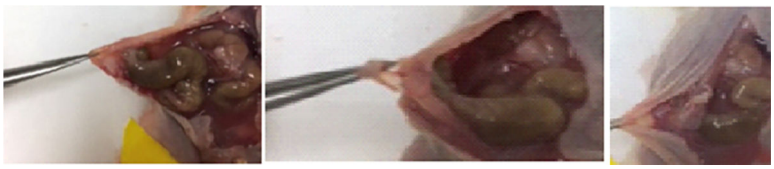

Figure 6.

Representative pictures of peritoneal adhesion in three ES-2-luc-bearing mice 21 days after surgery and insertion of empty sol–gels.

Table 1.

Cell Cytotoxicity of Paclitaxel and Rapamycin Individually and in Combination

cell type	ES-2-luc human ovarian cancer	ES-2-luc ascites mouse ovarian cancer	ES-2-luc-$PTX_{treated}$ ascites mouse ovarian cancer
IC_{50} of paclitaxel (nM)	119.2	136.5	193.9
IC_{50} of rapamycin (nM)	647.8	549.0	482.9
IC_{50} of paclitaxel/ rapamycin (nM)	130.3	53.6	65.5
combination index	0.6473	0.2451	0.2368

Table 2.

Median Survival of ES-2-luc-Bearing Xenograft Mice

formulation	empty disc	disc with paclitaxel and rapamycin	sol—gel with paclitaxel and rapamycin	empty sol—gel	control (no surgery and no treatment)
mean survival (days)	21	30	36	21	21

Table 3.

Physical Observation of the Sacrificed ES-2-luc- Bearing Mice

formulation	empty disc	disc with paclitaxel and rapamycin	sol—gel with paclitaxel and rapamycin	empty sol—gel	control (no surgery and no treatment)
peritoneal adhesion	no	no	no	yes	no
amount of peritoneal fluids	++	+	++	++	++++
color of peritoneal fluids	cloudy	straw or yellow	pinkish/cloudy	pinkish/cloudy	white/milky
tumor	solid	solid	solid	solid	solid, soft, liquid-like